

# The Magnetic Reconnection Induced Coherent Emission on Pulsars

Bi-Ping Gong\*

The pulsar radio emission mechanism remains an enigma since its discovery in 1967. The critical issue of origin of coherent emission is usually investigated separately from the micro-structure of individual pulses and characteristic emission frequency of pulsars... In this letter, these issues are interpreted in an unified scenario. The pulsar spin piles up magnetic field at the apex of last closed field line triggering magnetic reconnection. The resultant Alfvén wave interacts with open field lines giving rise to coherent maser curvature and cyclotron emission. Such a scenario of coherent emission not only imposes new limit to emission site, nanoburst, and characteristic frequency, but also affects polarization and pair production required in maintaining a marginal stable circuit in radio emission of pulsars.

## I. INTRODUCTION

Although an enormous observational data on pulsars and many models relating to the interpretation of the radio emission, but the critical issue on the origin of coherent emission is still an open question.

In early literature it was assumed to be emission by bunches[1]. Although such an assumption has been criticized[2], it remains implicit in more recent models, based on other types of bunches, i.e., solitons[3].

A more general aspect of origin of coherent emission is that a pulse profile is actually built up a large number of localized, transient events, which are described as: intermittency, fine structures, discrete emissions, short-lived emission centers, microstructure and nanoshots[4]. I.e., Crab pulsar exhibits GHz microbursts varying dramatically in less than a millisecond, which must be intrinsic to the radio emission process in the pulsar, since it is too rapid to be caused by propagation through turbulence in the Crab nebula or in the interstellar medium[5], which becomes more severe in the case of nanobursts[6]. Such bright nanobursts must be coherent, radiating in characteristic emission frequency, and then passing through a highly transparent medium to avoid being thermalized[7].

This letter exhibits a new scenario of coherency. The pulsar spin invokes centrifugal force driving plasma of closed field lines toward the light cylinder radius. As a result, the last closed field line is elongated and narrowed so is the current sheet formed by frozen plasma, which triggers rapid magnetic reconnection through chain of plasmoids responsible for nanoshots.

Such a nanoburst invokes coherent Alfvén wave (AW), its interaction with magnetic field of open field lines pump the coherent maser curvature and cyclotron emission at different pitch angles giving rise to O-mode and X-mode radiation.

Such scenario of maser emission triggered by AW stemming from reconnection near light cylinder naturally avoids difficulties in model of maser coherent emission originating in plasma instability[4].

Beside, as the reconnection always occurs at the end of last closed field line or the end of a current sheet, the subsequent radiation can propagate in the density cavity formed by tube of open field lines, which deviates from models of reconnection by coalescence of magnetic islands in the current sheet, where magnetic perturbations should propagate in the dense current sheet[8].

## II. THE RECONNECTION SITE AND COHERENCY

It occurs that starting the star with a surface charge and then releasing it will result in the positive particles from the equatorial zone simply popping out a short distance and being trapped by the intense closed magnetic field lines there [7, 9]. And such oblique dome-disc models are robust by detailed numerical modelling [10].

The frozen plasma trapped in closed field lines are driven by the centrifugal force toward the last field line. As a result, the magnetic field near light cylinder is enhanced significantly and magnetic reconnection is triggered in the last closed line region. The resultant release of free energy gives rise to seed of coherent wave. The process of wind up and relaxation repeat, so that the new last close field takes place of the previous one at the cost of both the rotation energy and magnetic energy of the pulsar.

The physics near the last closed field line or the separatrices can be described by the equation of motion of magnetohydrostatics,

$$\rho \frac{d\mathbf{v}}{dt} = -\nabla p + \mathbf{j} \times \mathbf{B} + \rho \mathbf{g} \quad (1)$$

where the current,  $\mathbf{j} = \nabla \times \mathbf{B}/\mu$ , can be simplified by  $j_y = \frac{1}{\mu} \frac{dB_z}{dx} = \frac{dB_z}{\delta}$  (where  $\delta$  is the thickness of the current layer) in the Cartesian coordinate as shown in Fig1a.

The centrifugal and gravitational acceleration on a particle,  $a = v^2/R$  and  $g = GM/R^2$ , are balanced at a radius of  $R_{eq}^3 = GM/\omega^2$ . Consequently, with  $R_{lc} = c/\Omega$  denoting the light cylinder radius, the centrifugal force overwhelms the gravity in the case of  $R \geq 10^{-1}R_{lc}$  for millisecond pulsars; and  $R \geq 10^{-2}R_{lc}$  for pulsars with spin period of a few seconds.

\* Also at Department of Physics, Huazhong University of Science and Technology

As the closed field lines where plasma frozen in extend to the light cylinder, Equation (1) is dominated by  $\rho v^2/R = |\mathbf{j} \times \mathbf{B}|$ . In other words, the centrifugal force is in equilibrium with centripetal force originating in magnetic tension near light cylinder,

$$\frac{B^2}{\mu R} = \rho \frac{v^2}{R} = \frac{j_y m_e}{e v'} \frac{v^2}{R} = \frac{B}{\mu \delta} \frac{m_e}{e v'} \frac{v^2}{R} \quad (2)$$

where  $m_e$  and  $e$  are mass and charge of an electron,  $v'$  is the speed of charge corresponding to the current  $j_y$ , which is parallel to the thickness direction,  $\delta$ , of the current layer as shown in Fig1a (  $L$  and  $b$  are the length and width of the sheet). Equation (2) can be further simplified as,

$$B \approx 10^{-3} \frac{c}{v'} \frac{1}{\delta} \quad (3)$$

Equation (3) indicates once magnetosphere is deformed to the extend of a small layer thickness,  $\delta$ , at the apex of last closed field lines, the magnetic field becomes much greater than that of the light cylinder  $B \gg B_{lc}$  where  $B_{lc} = B_s \left(\frac{R}{R_{lc}}\right)^3$ .

The effect of bent magnetic field lines as indicated by Equation (3) has been investigated as a critical role of ballooning instability in the near-Earth plasma sheet responsible for the onset of a substorm expansion [11]. The linear ballooning mode is unstable, and its nonlinear development leads to the formation of a series of plasmoids structures in the near-Earth and middle magnetotail regions of plasma sheet.

This model is support by experiment[12], in which a weak-external magnetic field in the direction perpendicular to the plasma propagation is applied, where the magnetic field is directly coupled with electrons. Since the kinetic pressure of plasma is much larger than the magnetic pressure, the magnetic field is distorted and locally anti-parallel. Plasma collimations, cusp and plasmoid like features with optical diagnostics are reported. Moreover, the plasmoid propagates at the electron Alfvén velocity, indicating a reconnection driven by the electron dynamics [12]. Such ballooning instability triggered reconnection is also consistent with simulated chain of plasmoids in pulsar magnetosphere[13].

The effect of magnetic diffusion at the reconnection site can be simplified by the combination of equation of induction, with the magnetic diffusivity,  $\eta$ ,

$$\frac{\partial \mathbf{B}}{\partial t} = \nabla \times (\mathbf{v} \times \mathbf{B}) + \eta \nabla^2 \mathbf{B} \quad (4)$$

and equation of motion as shown in Equation (1) (neglecting  $\nabla p$  and  $\rho g$ ). Making the usual wave assumption,  $\exp(-\omega_i t) \exp(i\omega_r t)$ , a simple dissipation relation is obtained[14],

$$\omega^2 = k^2 v_A^2 - i\omega \frac{kv_A}{R_m}, \quad (5)$$

where  $R_m$  is the magnetic Reynolds number.

In such a case, the frequency of corresponding AW can be estimated by the plasmoid size of  $\lambda \sim \delta \sim 10^{-2} \text{m}$  under the magnetic field of strength,  $B \sim 10^4 \text{T}$  as shown in Equation (3). The wave frequency,  $\omega_r \approx kv_A$ , corresponds to a time scale of,

$$\tau_r = \frac{2\pi}{\omega_r} \sim 2\pi \left(\frac{\lambda}{1 \times 10^{-2}}\right) \left(\frac{3 \times 10^8}{v_A}\right) \sim 2 \times 10^{-10} \text{s} \quad (6)$$

On the other hand, the damping of such an AW is determined by  $\omega_i = -kv_A/(2R_m)$ , so that

$$\tau_i = \frac{2\pi}{\omega_i} \sim 2\pi \mu_0 \left(\frac{\lambda}{1 \times 10^{-2}}\right)^2 \left(\frac{1}{\eta}\right) \sim 8 \times 10^{-10} \text{s} \quad (7)$$

Consequently, Equation (6) and Equation (7) predict a wave train of length,  $s \sim \tau_i c \sim 2 \times 10^{-1} \text{m}$ , wave number,  $k \sim 1/\delta \sim 10^2$ , and hence,  $ks \sim 20 \gg 1$ , which corresponds to a GHz nanoburst of short frequency range,  $\Delta\omega/\omega \sim 0.03$  comparable to a typical FRB.

The required rapid reconnection can be achieved by a new last closed field line (b) catching up the old one (a) as shown in Fig1a, which leads to rapid reconnection of plasmoids. As a result, such reconnection alway occurs at the end of the current sheet.

Moreover, pair production can be triggered in the diffusing region, where half plasma eject out contributing to the pulsar wind; and the other half return to the pulsar surface along separatrices consisting with simulations[15].

The duration of a microstructure much shorter than a nanoburst is constrained by both the characteristic frequency of GHz and the coherent condition,  $ks \gg 1$ . And a microstructure much longer than a nanoburst is restricted either, because a much longer time scale,  $\tau_i$ , would require a much smaller magnetic diffusivity,  $\eta$ , in Equation (7) which prevents rapid reconnection and pair production from happening. Therefore, the characteristic frequency, nanoburst and magnetic field at light cylinder as shown in Equation (3) are closely related in the context of reconnection induced radio emission.

The coherency of outward AW interacting with magnetic field can be analyzed by energy radiated per unit solid angle per unit frequency interval from a bunch with length  $L$  and  $N$  particle moving along a curved field line[16],

$$\frac{dI_N}{d\omega d\Omega} = \frac{dI}{d\omega d\Omega} F_\omega(N) \quad (8)$$

where  $F_\omega(N)$  is a dimensionless parameter denoting the enhancement factor due to coherence defined,

$$F_\omega(N) = |\sum_j^N e^{-i\omega(\mathbf{n} \cdot \Delta \mathbf{r}_j/c)}|^2 \quad (9)$$

where,  $\mathbf{n}$  is the unit vector to the observer, and  $\Delta \mathbf{r}_j$  is a section of the bunch length  $L$ . For a non-coherent bunch of length  $L$ , only if all electrons are at one point,  $\Delta r_j = 0$ , can one get  $F_\omega(N) = N^2$ .

In contrast, the AW of wave length,  $\lambda \sim \delta \sim 1 \times 10^{-2} \text{m}$ , and a coherent length  $L_i \sim c\tau_i \sim 2 \times 10^{-1} \text{m}$  corresponds

to a wave train of length,  $\sum \Delta r_j = \sum \lambda = L_i \sim 20\lambda$ , under an uniform distribution of electrons (positrons) of a number of  $N$  along  $L_i$ . Then simply applying the half wave superposition, the enhancement factor of the whole length  $L_i$  yields  $F_\omega(N_i) = N_i^2$ , which ensures the coherency of a nanoburst.

On the other hand, as proposed [6], microbursts are incoherent superpositions of short-lived narrowband, nanoshots, and all microbursts are clumps of nanoshots. In such a scenario, the broadband of each such microburst can be interpreted by the wide frequency range of the centre frequencies of the nanoshots (each is short in frequency range) in a microburst[6].

In the context of Sweet-Parker reconnection, with a current sheet of length  $L$  and thickness  $\delta$ , conservation of mass implies,

$$Lv_i = \delta v_{Ai} \quad (10)$$

As the reconnection region corresponds to a diffusion speed of,  $v_i = \eta/\delta \sim 10^2 \text{ m/s}$  with parameters adopted in Equation (7), we have a layer length of  $L \sim 10^4 \text{ m}$ , which composes numerous nanoshots stemming from fast reconnection of plasmoids at the end of such a sheet. The swing of such a dynamic current sheet through a pulse window results in the single pulse of a pulsar, which corresponds to an enhancement factor of Equation (9) of,

$$F_\omega(N_i, N) = NN_i^2 \quad (11)$$

where  $N_i$  and  $N$  are number of particles in a nanoburst and number nanoshots in a single pulse respectively. This explains why the single pulse of a pulsar appears much dimmer than a nanoburst.

### III. WAVES AND CIRCUIT

The energetic electrons and positrons injected out of the reconnection site with velocity  $\mathbf{v}$  as discussed in last section undergo resonant wave-particle interaction,  $\omega - \mathbf{k} \cdot \mathbf{v} = \mathbf{0}$ , in an unmagnetized plasma. Such a relation can be applied to the central of the open field lines (zero pitch angle) as shown in Fig1b where the strength of surrounding magnetic field chancels out. The coherence of such a AW is ensured by Equation (6) and Equation (7).

In the case of larger pitch angles as shown in Fig1b, the AW interacts with surrounding open field lines giving rise to coherent cyclotron and curvature emission. As the interaction time scale is much shorter than that of coherence time of Equation (7),  $\tau \sim \hbar/(\gamma m_e c^2) \ll 1 \text{ ns}$ , the coherence of such a seed AW is actually undisturbed by further cyclotron and curvature processes, whereas their polarizations are affected profoundly.

The propagation of reconnection induced AW in magnetic field can energize electrons resulting in a new cyclotron maser instability with time scale indicated by

Equation (6) and Equation (7). The resonance condition in the presence of magnetic field is read,

$$\omega = s\Omega_e/\gamma + k_\parallel v_\parallel \quad (12)$$

The right hand side of Equation (12) corresponds to an effective cyclotron phase angle advances at the rate of the effective cyclotron frequency,  $\Omega_{eff} = s\Omega_e/\gamma + k_\parallel v_\parallel$ . Resonance takes place when the electron (positron) remains in phase with the wave. In other words, the interaction of Equation (12) is equivalent to lifting the electrons collectively into higher level providing sufficient free energy to induce a substantially intense coherent radiation.

The influence of AWs on the maser emission in coronal loops has also calculated in detail[17–19], which shows that the AW can qualitatively affect the velocity distribution of energetic electrons via pitch-angle scattering and at the same time they can also modify the usual cyclotron resonance processes. As a result, the O mode emission is effectively amplified further by AWs while the X mode emission is hardly affected.

On the other hand, with  $s = 1$  and  $\Omega_c = \Omega_e$ , the right hand side of Equation (12) can also describe the effective curvature phase angle advances at the rate of the effective curvature frequency,  $\Omega_{eff} = \Omega_c/\gamma + k_\parallel v_\parallel$ , so that AW affected curvature emission can be studied in a similar approach. The relative energy density between the cone and core as well as corresponding polarization depends on the ratio of energy density of cyclotron and curvature maser emission which awaits further investigation.

At the reconnection site, both the outflow and inward beams are accelerated by the reconnection electrical field near X line. The presence of guided field in the X line region of the reconnection site leads to strongly field aligned distribution of beams of electron and positron[20]. One pair of electron and positron return to the pulsar directly along separatrices of the X line, as shown in Fig1b. Correspondingly, the other pair of energetic electron and positron beams move along opposite pair of separatrices of the X line away from the pulsar, most of which contribute to the pulsar wind. As a result, a net loss of charged particles in such a process is inevitable. Fortunately, the pair production addressed at the end of last section provides additional charge supply to the circuit as shown in Fig1c, so that the whole process can proceed in a marginal stable circuit.

As shown in Fig1bc, the return current is similar to both the simulated configuration of the electric charge and the electric current of the equatorial current sheet[15]; and the current configuration responsible for aurora observed by the satellite passing through the acceleration region [21]. The return current formed by downward pair of electron and positron can screen the inductive electric field at pulsar surface (in the case of charge starving) with a circuit as shown in Fig1c.

A simple and unified scenario on where and how coherent radio emission is proposed in this letter, which naturally relates coherency, microstructure, characteristic frequency, emission site, density cavity, circuit, and

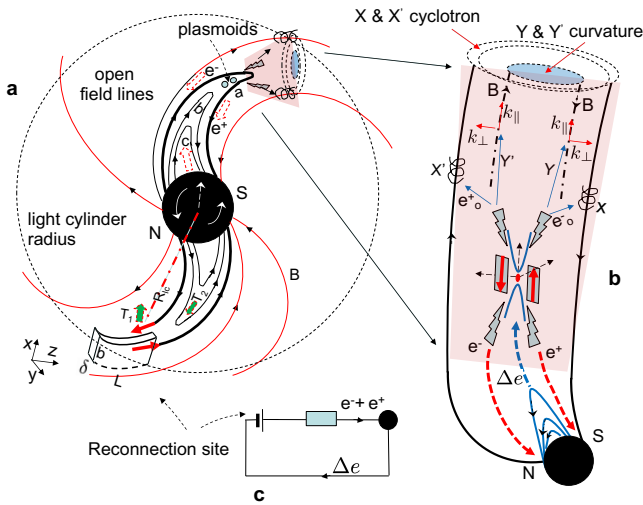


FIG. 1. The schematic configuration of reconnection induced radio emission. Panel a: spin deformed last closed field lines surrounded by open field line tubes. Small circles denote plasmoids inside the upper last closed field line, their annihilation gives rise to outward emission and return current (dotted arrows). The current sheet is shown at bottom of the spiral. Panel b: reconnection site with guided field which separates the electron and positron beams. The outward beams interact with the open field lines invoking maser emission. And the return beams contribute to the circuit as shown in Panel c.

polarization of a pulsar.

[1] G. Benford and R. Buschauer, Coherent pulsar radio radiation by antenna mechanisms: general theory., *Monthly Notices of the Royal Astronomical Society* **179**, 189 (1977).

[2] D. B. Melrose, Maser pulse emission mechanisms, in *Pulsars: 13 Years of Research on Neutron Stars*, Vol. 95, edited by W. Sieber and R. Wielebinski (1981) pp. 133–139.

[3] J. Gil, Y. Lyubarsky, and G. I. Melikidze, Curvature Radiation in Pulsar Magnetospheric Plasma, *Astrophys. J.* **600**, 872 (2004), arXiv:astro-ph/0310621 [astro-ph].

[4] D. Melrose, Pulse Emission Mechanisms, in *Young Neutron Stars and Their Environments*, Vol. 218, edited by F. Camilo and B. M. Gaensler (2004) p. 349, arXiv:astro-ph/0308471 [astro-ph].

[5] J. H. Crossley, J. A. Eilek, T. H. Hankins, and J. S. Kern, Short-lived Radio Bursts from the Crab Pulsar, *Astrophys. J.* **722**, 1908 (2010), arXiv:1009.0735 [astro-ph.HE].

[6] J. A. Eilek and T. H. Hankins, Radio emission physics in the Crab pulsar, *Journal of Plasma Physics* **82**, 635820302 (2016), arXiv:1604.02472 [astro-ph.HE].

[7] F. C. Michel and H. Li, Electrodynamics of neutron stars, *Physics Reports* **318**, 227 (1999).

[8] Y. Lyubarsky, Radio emission of the Crab and Crab-like pulsars, *Monthly Notices of the Royal Astronomical Society* **483**, 1731 (2019), arXiv:1811.11122 [astro-ph.HE].

[9] E. A. Jackson, A new pulsar atmospheric model. I. Aligned magnetic and rotational axes., *Astrophys. J.* **206**, 831 (1976).

[10] A. Spitkovsky, Electrodynamics of Pulsar Magnetospheres, in *Young Neutron Stars and Their Environments*, Vol. 218, edited by F. Camilo and B. M. Gaensler (2004) p. 357, arXiv:astro-ph/0310731 [astro-ph].

[11] P. Zhu and J. Raeder, Ballooning instability-induced plasmoid formation in near-Earth plasma sheet, *Journal of Geophysical Research (Space Physics)* **119**, 131 (2014).

[12] Y. Kuramitsu, T. Moritaka, Y. Sakawa, T. Morita, T. Sano, M. Koenig, C. D. Gregory, N. Woolsey, K. Tomita, H. Takabe, Y. L. Liu, S. H. Chen, S. Matsukiyo, and M. Hoshino, Magnetic reconnection driven by electron dynamics, *Nature Communications* **9**, 5109 (2018).

[13] H. Hakobyan, A. Philippov, and A. Spitkovsky, Reconnection and high energy radiation in the outer magnetospheres of gamma-ray emitting pulsars, in *APS Division of Plasma Physics Meeting Abstracts*, APS Meeting Abstracts, Vol. 2019 (2019) p. NP10.044.

[14] *Saas-Fee Advanced Course 24: Plasma Astrophysics* (1994).

[15] I. Contopoulos, J. Pétri, and P. Stefanou, Hybrid numerical simulations of pulsar magnetospheres, *Monthly Notices of the Royal Astronomical Society* **491**, 5579 (2020), arXiv:1909.13504 [astro-ph.HE].

[16] Y.-P. Yang and B. Zhang, Bunching Coherent Curvature Radiation in Three-dimensional Magnetic Field Geometries, *Journal of Plasma Physics* **85**, 8508501 (2019).

try: Application to Pulsars and Fast Radio Bursts, *Astrophys. J.* **868**, 31 (2018), arXiv:1712.02702 [astro-ph.HE].

[17] C. S. Wu, C. B. Wang, D. J. Wu, and K. H. Lee, Resonant wave-particle interactions modified by intrinsic Alfvénic turbulence, *Physics of Plasmas* **19**, 082902 (2012).

[18] G. Q. Zhao, L. Chen, and D. J. Wu, Solar Type III Radio Bursts Modulated by Homochromous Alfvén Waves, *Astrophys. J.* **779**, 31 (2013).

[19] G. Q. Zhao, H. Q. Feng, D. J. Wu, L. Chen, J. F. Tang, and Q. Liu, Cyclotron Maser Emission from Power-law Electrons with Strong Pitch-angle Anisotropy, *Astrophys. J.* **822**, 58 (2016), arXiv:1603.01923 [astro-ph.SR].

[20] P. L. Pritchett, Relativistic electron production during guide field magnetic reconnection, *Journal of Geophysical Research (Space Physics)* **111**, A10212 (2006).

[21] R. E. Ergun, C. W. Carlson, J. P. McFadden, G. T. Delory, R. J. Strangeway, and P. L. Pritchett, Electron-Cyclotron Maser Driven by Charged-Particle Acceleration from Magnetic Field-aligned Electric Fields, *Astrophys. J.* **538**, 456 (2000).